# Reorientation of a Nonspherical Capsule in Creeping Shear Flow

Toshihiro Omori,[1,*] Yohsuke Imai,[2] Takami Yamaguchi,[1] and Takuji Ishikawa[2,†]

[1]*Department of Biomedical Engineering, Tohoku University, Aoba 6-6-01 Sendai Miyagi, Japan*
[2]*Department of Bioengineering and Robotics, Tohoku University, Aoba 6-6-01 Sendai Miyagi, Japan*

(Received 24 August 2011; published 28 March 2012)

The dynamics of a capsule and a biological cell is of great interest in chemical engineering and bioengineering. Although the dynamics of a rigid spheroid is well understood by Jeffery's theory, that of a spheroidal capsule remains unclear. In this Letter, the motion of a spheroidal capsule or a red blood cell in creeping shear flow is investigated. The results show that the orientation of a nonspherical capsule is variant under time reversal, though that of a rigid spheroid is invariant. Surprisingly, the alignment of a nonspherical capsule over a long time duration shows a transition depending on the shear rate, which can be utilized for a particle-alignment technique. These findings form a fundamental basis of the suspension mechanics of capsules and biological cells.

DOI: 10.1103/PhysRevLett.108.138102 PACS numbers: 47.63.mf, 83.50.−v, 87.16.D−

About a century ago, Jeffery analytically derived the motion of a nonspherical object in creeping linear background flow [1]. Since then, Jeffery's theory has been used to describe the alignment of rods and ellipsoids, such as bacteria, platelets, etc. The theory states that the trajectory of a non-Brownian rigid ellipsoid in Stokes flow is invariant under time reversal and that reorientation over a long time duration does not occur under simple shear flow conditions. The time reversibility can be destroyed by introducing inertia effects [2] or viscoelastic properties of the surrounding fluid [3], because the motion is no longer independent of time in these cases. However, the effect of particle deformability on the time reversibility is not well clarified. This study investigates this question by using a capsule as a model deformable object.

A capsule is a liquid drop enclosed by a deformable membrane, which is of great interest in the chemical engineering, bioengineering, and food industries. Many capsules in realistic situations are not perfect spheres because of the inhomogeneity of the membrane properties or folding due to unbalanced osmotic pressure. If one places a nonspherical capsule in creeping shear flow, how does the orientation change relative to the flow field over a long time duration? Jeffery speculated that an ellipsoid may alter its orientation so that the viscous energy dissipation of the system becomes minimal [1]. However, this may not be true for a capsule with a large deformation. Although many former studies have examined the dynamics of a nonspherical capsule [4–8], none of them can answer this question.

In this Letter, the motion of a non-Brownian spheroidal capsule or a red blood cell (RBC) in creeping shear flow is investigated numerically. The results show that the orientation of a nonspherical capsule is variant under time reversal, although the orientation of a rigid ellipsoid is invariant. Surprisingly, the alignment of a nonspherical capsule over a long time duration shows a transition depending on the shear rate. The transition cannot be explained by the minimum energy dissipation, as speculated by Jeffery; the full fluid and solid mechanics are necessary to understand this phenomenon. The obtained results can be utilized for particle-alignment techniques in engineering applications and shed light on the complex dynamics of capsules and biological cells.

A capsule is assumed to be filled with an incompressible Newtonian fluid of viscosity $\lambda\mu$ and freely suspended in another fluid with the same density but viscosity $\mu$. When the thickness of the capsule wall is small compared to its size and radius of curvature, the membrane can be modeled as a 2D hyperelastic surface without bending rigidity. In this study, we use two kinds of constitutive laws for the membrane: the neo-Hookean (NH) law [9] and the Skalak (SK) law [10]. The NH law describes isotropic volume-incompressible rubberlike material properties, whereas the Skalak law expresses the area incompressibility of a biological membrane.

To calculate capsule deformation accurately, fluid-structure interactions between the motion of the internal and external fluids and that of the capsule membrane have to be solved precisely. We assume that the flow is Stokesian, i.e., inertia-free, and the flow field is solved by a boundary element method. A finite element method is employed to solve the membrane mechanics. The governing equations and numerical methods are the same as in Refs. [6,11], and the details are explained in Ref. [12]. The reference shape of the capsule is assumed to be spheroid or biconcave, in the same manner as in Refs. [5,6]. The aspect ratio between the principal axes of the spheroid is represented by $\alpha$. A linear triangular mesh with 5120 elements is used to discretize the membrane. The validation of the numerical methods is presented in Ref. [12].

In a Cartesian reference frame with the capsule center as the origin, the undisturbed linear background flow $\mathbf{v}^{\infty}$ can be described as $\mathbf{v}^{\infty} = (\mathbf{E} + \mathbf{\Omega}) \cdot \mathbf{x}$, where $\mathbf{E}$ and $\mathbf{\Omega}$ are the

 

rate of strain and rotation tensors, respectively. In this study, we use two types of background flow: (a) a simple shear flow given by $E_{xy} = E_{yx} = \Omega_{xy} = -\Omega_{yx} = \frac{\dot{\gamma}}{2}$ (all the other components = 0), as shown in Fig. 1(a), and (b) an oscillatory planar elongational flow given by $E_{xy} = E_{yx} = \frac{\dot{\gamma}}{2}\cos\omega t$ (all the other components = 0), as shown in Fig. 1(b). Here, $\dot{\gamma}$ is the shear rate or the elongational rate, $t$ is the time, and $\omega$ is the angular velocity of the flow, which is correlated to the oscillation period $T$ as $T = 2\pi/\omega$. The capillary number Ca represents the ratio of the viscous force to the elastic force and is given by $\mathrm{Ca} = \mu\ell\dot{\gamma}/G_s$, where $G_s$ is the membrane shear modulus and $\ell$ is the radius of a sphere that has the same volume as the ellipsoid or the biconcave capsule.

We first investigate the motion of a spheroidal oblate capsule in simple shear flow and compare the results with those of a rigid spheroid. To examine the capsule orientation efficiently, we define the orientation vector **e** as a unit vector extending from the center of gravity and pointing to material point $P$ located at the revolution axis of the unstressed spheroidal capsule. $\theta$ is defined as the angle between **e** and the $z$ axis, as shown in Fig. 1(c). At time $t = 0$, the oblate capsule without prestress is placed at an initial angle $\theta_0$ of $\pi/4$. The deformation at time $t > 0$ due to the background shear is calculated until the steady periodic motion is achieved.

The motions of an oblate capsule with Ca = 0.3 and 1.0 are shown in Fig. 2(a) and 2(b), respectively ($\alpha = 0.6$, $\lambda = 1$, and NH membrane). The time history of $\theta$ is also shown in Fig. 2(c) for 30 periods of rotation. The results of a rigid spheroidal with the same $\alpha$ [1] are also plotted in the figure for comparison. Because of the nonspherical reference shape of the capsule membrane, $\theta$ oscillates twice during one rotation. In addition to the short-time oscillation, $\theta$ tends to approach towards 0 or $\pi/2$, depending on Ca, over a long time duration. The reorientation of the capsules is also clear in observing Figs. 2(a) and 2(b), because the material point $P$, which is indicated as a blue dot in the figures, moves towards $z = 0$ when Ca = 0.3, whereas it moves towards the $z$ axis when Ca = 1.0. We note that the final orientation is independent of the initial orientation; this was confirmed numerically by changing the initial orientation randomly. Such reorientation did not happen for a rigid spheroid, as shown in Fig. 2(c). These results clearly illustrate that a deformable capsule becomes reoriented, even in simple shear flow, and the time reversibility of Jeffery's orbit can be destroyed by introducing particle deformability.

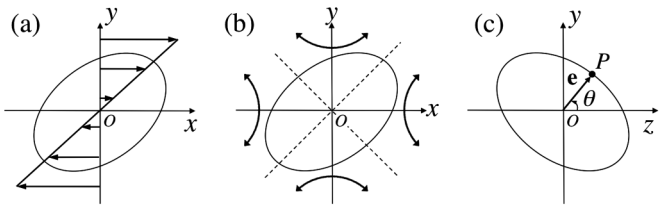


FIG. 1. Schematic illustration of a capsule in (a) simple shear flow and (b) oscillating planar elongational flow. (c) Orientation vector **e** is defined as a unit vector extending from the center of gravity and pointing to material point $P$. $\theta$ is defined as the angle between **e** and the $z$ axis.

The results of Fig. 2 raise another important question about why the reorientation direction shows a transition with increasing Ca. We calculated the viscous energy dissipation due to the capsule motion to determine whether the transition occurred to minimize the dissipation energy. However, we did not observe a one-to-one correlation between the capsule reorientation and the minimum energy dissipation. Thus, the full fluid and solid mechanics must be examined to answer this question.

To understand the basic mechanism of the transition, we further simplify the background flow field by deleting the rotational contribution from the shear flow. When an oblate capsule with an arbitrary initial orientation is subjected to steady planar elongational flow, the orientation is finally directed towards the compressing direction in all cases. Given that the reorientation transition does not appear in steady planar elongational flow, the unsteadiness in the flow field likely plays an important role in the transition.

Next, we apply oscillatory planar elongational flow, given by Fig. 1(b), to an oblate capsule. In this flow field, the elongational rate and changing frequency of the elongational direction can be independently controlled. At $t = 0$, the oblate capsule without prestress is placed at $\theta_0 = \pi/4$. The capsule motions for the second period of oscillation with $\omega/(\dot{\gamma}\pi) = 0.08$ and Ca = 0.3 and 1.0 are shown in Figs. 3(a) and 3(b) ($\alpha = 0.6$, $\lambda = 1$, and NH

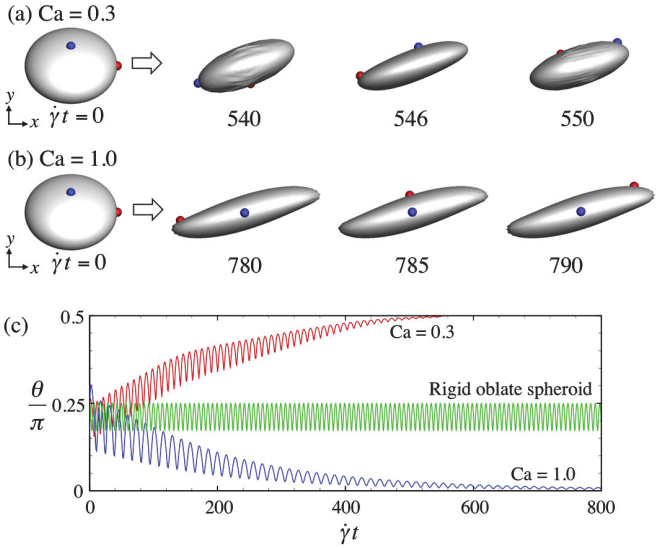


FIG. 2 (color). Oblate capsule in a simple shear flow with (a) Ca = 0.3 and (b) 1.0 ($\alpha = 0.6$, $\lambda = 1$, and NH membrane). Blue and red dots are material points on the membrane and are plotted as tracers. (c) Time change of $\theta$, where the result of a rigid spheroid with same $\alpha$ [1] is also plotted for comparison.

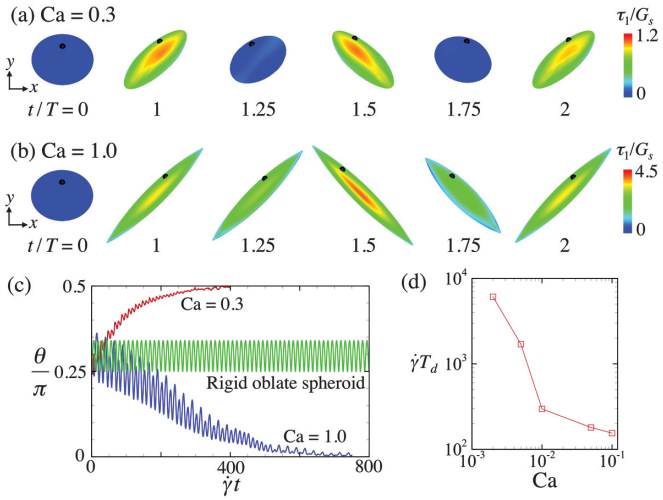


FIG. 3 (color). Motion of an oblate capsule in oscillating planar elongational flow with $\omega/(\dot{\gamma}\pi) = 0.08$ and (a) Ca = 0.3 or (b) Ca = 1.0 ($\alpha = 0.6$, $\lambda = 1$, and NH membrane). A black dot is placed at $P$ as a tracer. (c) Time change of $\theta$, where the result of a rigid spheroid with the same $\alpha$ [1] is plotted for comparison. (d) Dimensionless drift time in the small Ca regime.

membrane). Color contours show the distribution of $\tau_1$, where $\tau_i$ is the in-plain principal elastic tension and $\tau_1 \geq \tau_2$. The time history of $\theta$ is also shown in Fig. 3(c) for 30 periods of oscillation. When Ca = 0.3, $\theta$ approaches to $\pi/2$ after a sufficient time duration, whereas when Ca = 1.0, $\theta$ approaches to 0. For Ca = 0.3, the capsule deformation is small at $t/T = 1.25$ and 1.75, when there is no background flow, and the $\tau_1$ distributions at $t/T = 1.0$ and 1.5 are similar. For Ca = 1.0, however, large deformations remain at $t/T = 1.25$ and 1.75, resulting in a strong asymmetry in the $\tau_1$ distribution between $t/T = 1.0$ and 1.5. Thus, the deformation is strongly affected by the time history in the high Ca regime, whereas it is quasisteady in the low Ca regime. This qualitative difference in the tension distribution likely causes the reorientation transition. When Ca is very small, the capsule should behave like a rigid body. In order to confirm the convergence, we calculate drift time $T_d$ required for drifting from $\theta = \pi/4$ to $\pi/2$ and plot it in Fig. 3(d). We see that $\dot{\gamma}T_d$ increases rapidly as Ca is decreased, indicating convergence to the rigid body motion.

To clarify the reorientation phenomena in more detail, we plot a phase diagram of the final orientation as a function of Ca and $\omega/\dot{\gamma}\pi$. The oblate capsule is again subjected to the oscillatory planar elongational flow with $\theta_0 = \pi/4$. The computation is carried out for $N$ periods of oscillation, and $N$ is set to 30, as in Fig. 3(c). The convergence of the final angle is determined by the following equation: $|\theta_{30} - \theta_f| \leq \epsilon$, where $\theta_{30}$ is the average orientation vector of the 30th rotation, and $\theta_f = 0$, $\pi/2$, or $\theta_0$. The threshold value of $\epsilon = 0.05$ is used in this study, because the results with $\epsilon = 0.1$ and 0.05 are almost the same. When the convergence criteria is not satisfied, we determined that the reorientation is in the transit regime.

The results of the phase diagram are shown in Fig. 4. The red region ($\theta_{30} \approx \theta_0$) indicates the rigid body motion or high frequency oscillation. When $\omega$ is very large, the capsule has little time to deform, which results in no obvious reorientation. When Ca $\rightarrow$ 0, the capsule motion converges to the rigid body motion. Figure 3(d) indicates that the red region also appears in the Ca $< 0.001$ regime when $\omega/\dot{\gamma}\pi = 0.08$, though the diagram in this small Ca region is not plotted due to extremely high computational load. The green region ($\theta_{30} \approx \pi/2$) indicates the quasisteady deformation. This region appears when $\omega$ is small, including the steady planar elongation ($\omega = 0$). The magenta region indicates infinite stretching. This region appears only when the membrane is strain-softening, such as NH membrane. A strain-hardening membrane can avoid this problem [13]. The black region ($\theta_{30} \approx 0$) indicates large unsteady deformation. This region appears only when the capsule is subjected to the large elongation with the moderate oscillating frequency. The phase diagram may be slightly affected by the selection of $N$. Since $N$ is limited in terms of the computational cost, we cannot technically increase $N \rightarrow \infty$. These results clearly illustrate that the convergence of $\theta \rightarrow 0$ appears only when the large deformation is affected by the time history.

In the case of shear flow, the elongational direction relative to the material point on the membrane oscillates with the angular velocity of the membrane motion. Thus, one may assume $\omega$ as the average rotational velocity of a capsule in shear flow and draw the curve shown in Fig. 4. The results of an oblate capsule in shear flow, shown in Fig. 2, are plotted in Fig. 4 by circles. A curve with small

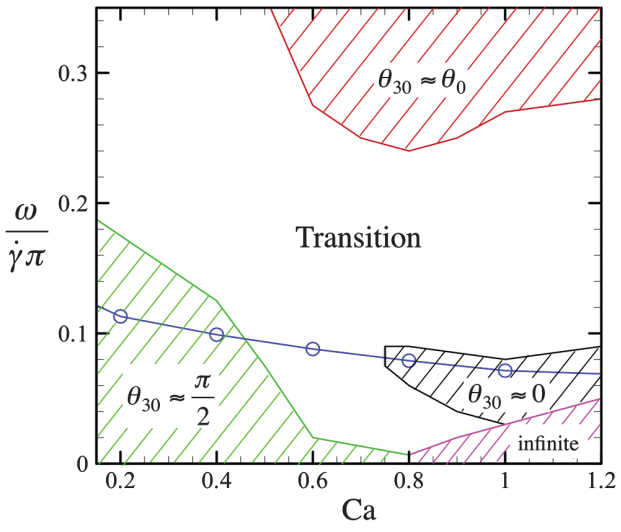


FIG. 4 (color). Phase diagram of the oblate capsule in oscillating elongational flow ($\alpha = 0.6$, $\lambda = 1$, and NH membrane). The circles in the figure indicate the converted results of the shear flow case.

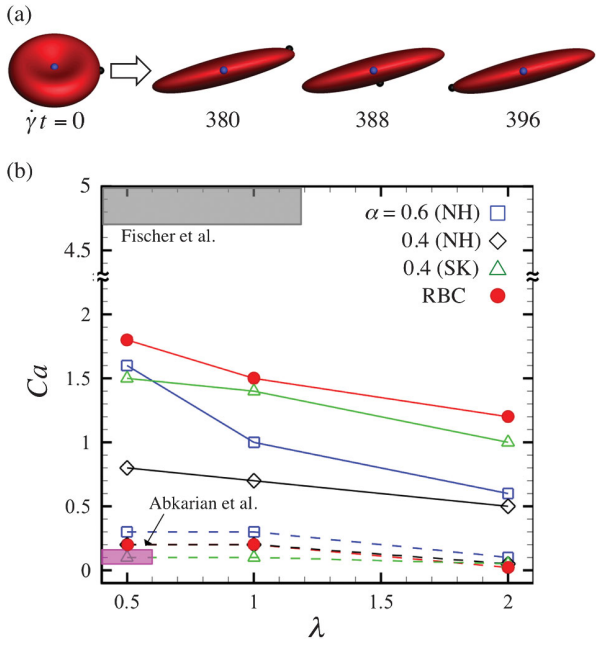


FIG. 5 (color). (a) Motion of a RBC in shear flow (Ca = 2.0, $\lambda = 1.0$). Blue and black dots are material points on the membrane and are plotted as tracers. (b) Effects of $\lambda$ on the critical Ca number of oblate capsules and a RBC. The solid lines in the figure indicate $Ca_0$, and the broken lines indicate $Ca_{\pi/2}$. Experimental conditions of Refs. [7,8] are plotted by gray and magenta regions, respectively.

Ca exists in the $\theta \to \pi/2$ region, whereas a curve with large Ca exists in the $\theta \to 0$ region. These results indicate that the reorientation transition found in the shear flow can also be explained by using Fig. 4.

Finally, we investigate the reorientation of a RBC in shear flow. The RBC membrane is modeled by the SK law with $C = 10$, where $C$ is the ratio of area dilation to the shear modulus. Here we also investigate the effect of the viscosity ratio $\lambda$. Initially, the RBC is set to $\theta_0 = \pi/4$. The results of Ca = 2 and $\lambda = 1$ are shown in Fig. 5(a). Material point $P$, indicated as a blue dot in the figure, shifts to the $z$ axis, i.e., $\theta \to 0$, for large Ca. When Ca was small, on the other hand, we confirmed that $\theta \to \pi/2$ in the same manner as the spheroidal capsule (data not shown). When $\theta = 0$, the RBC membrane has a pure tank-treading motion, and the membrane no longer oscillates during the rotation. When $\theta \neq 0$, on the other hand, the RBC shows a swinging motion, and the membrane oscillates during the rotation.

To effectively discuss the effect of $\lambda$ and the constitutive law on the reorientation transition in shear flow, we define critical values of Ca: $Ca_{\pi/2}$ indicates the maximum Ca value to show $\theta_{30} \approx \pi/2$ convergence, and $Ca_0$ indicates the minimum Ca value to show $\theta_{30} \approx 0$ convergence. The results of a RBC as well as spheroidal capsules with $\alpha = 0.4$ and 0.6 and with two types of membrane constitutive laws are shown in Fig. 5 as a function of $\lambda$. $Ca_{\pi/2}$ and $Ca_0$ tend to decrease as $\lambda$ increased. This is because the time history of deformation remains for a longer time as the inside viscosity increased, which leads to the transition in the smaller Ca conditions. The figure also indicates that the effect of the constitutive law is considerable. A capsule with the SK membrane tends to have a larger critical $Ca_0$ than that with the NH membrane. This is because the SK law shows the strain-hardening property, whereas NH law shows the strain-softening, so large deformations are suppressed by the SK membrane. Thus, the reorientation transition can be understood by considering the fluid and solid mechanics of capsule deformation.

In Fig. 5, experimental conditions of Refs. [7,8] are plotted by gray and magenta regions, respectively, by assuming $\mu = 11$–$59$ mPa · s, $\dot{\gamma} = 800\ s^{-1}$ for Ref. [7] or 22–47 mPa · s and $\dot{\gamma} = 5\ s^{-1}$ for Ref. [8], and $G_s = 4\ \mu$N/m and $\ell = 2.82\ \mu$m for both cases. We see the experimental conditions of Ref. [7] are above $Ca_0$, where our model shows the pure tank-treading motion as in Ref. [7]. The experimental conditions of Ref. [8] are below $Ca_{\pi/2}$, where our model shows the swinging motion as in Ref. [8]. Thus, the present results can nicely explain the difference of two former experimental observations by Refs. [7,8], even without introducing any inertial effect. We also note that the phase transition during reorientation is observed for a prolate spheroidal capsule, although the results are not included here. Thus, the reorientation transition is robust regardless of the reference shape of the capsule.

The results obtained in this study illustrate that the reorientation transition appears in a wide variety of artificial and biological capsules. Given that the transition can be controlled by adjusting the background flow strength as well as the unsteadiness in the background flow direction, the results obtained here can be utilized for particle-alignment techniques in engineering applications, such as counting nonspherical particles by light scattering, making anisotropic materials, etc. These findings form a fundamental basis for the suspension mechanics of capsules and biological cells.

We are grateful for helpful discussions with D. Barthès-Biesel and A.-V. Salsac of Université de Technologie de Compiègne.

*omori@pfsl.mech.tohoku.ac.jp
†ishikawa@pfsl.mech.tohoku.ac.jp

[1] G. Jeffery, Proc. R. Soc. A **102**, 161 (1922).
[2] Z. Yu, N. Phan-Thien, and R. Tanner, Phys. Rev. E **76**, 026310 (2007).
[3] Y. Iso, D. Koch, and C. Cohen, J. Non-Newtonian Fluid Mech. **62**, 115 (1996).
[4] P. Bagchi and R. Kalluri, Phys. Rev. E **80**, 016307 (2009); D. Le and S. Wong, J. Comput. Phys. **230**, 3538 (2011); S. Kessler, R. Finken, and U. Seifert, J. Fluid Mech. **605**, 207

(2008); P. M. Vlahovska, Y.-N. Young, G. Danker, and C. Misbah, J. Fluid Mech. **678**, 221 (2011); J. M. Skotheim and T. W. Secomb, Phys. Rev. Lett. **98**, 078301 (2007); Y. Sui, Y. T. Chew, P. Roy, X. B. Chen, and H. T. Low, Phys. Rev. E **75**, 066301 (2007).

[5] S. Ramanujan and C. Pozrikidis, J. Fluid Mech. **361**, 117 (1998).

[6] J. Walter, A.-V. Salsac, and D. Barthès-Biesel, J. Fluid Mech. **676**, 318 (2011).

[7] T. Fischer, M. Stohr-Lissen, and H. Schmid-Schonbein, Science **202**, 894 (1978).

[8] M. Abkarian, M. Faivre, and A. Viallat, Phys. Rev. Lett. **98**, 188302 (2007).

[9] A. E. Green and J. E. Adkins, *Large Elastic Deformations* (Clarendon, Oxford, 1970), 2nd ed.

[10] R. Skalak, A. Tozeren, R. P. Zarda, and S. Chien, Biophys. J. **13**, 245 (1973).

[11] E. Foessel, J. Walter, A.-V. Salsac, and D. Barthès-Biesel, J. Fluid Mech. **672**, 477 (2011); T. Omori, T. Ishikawa, D. Barthès-Biesel, A.-V. Salsac, J. Walter, Y. Imai, and T. Yamaguchi, Phys. Rev. E **83**, 041918 (2011).

[12] See Supplemental Material at http://link.aps.org/supplemental/10.1103/PhysRevLett.108.138102 for movies.

[13] W. R. Dodson III and P. Dimitrakopoulos, Phys. Rev. Lett. **101**, 208102 (2008).